Basal slip latent hardening by prism plane slip dislocations in sapphire (α-Al_2O_3)

M. Castillo Rodríguez*,**, A. Muñoz**, J. Castaing***, P. Veyssière**** and A. Domínguez-Rodríguez**

*Max-Planck-Institut für Metallforschung, StEM, Heisenbergstr. 3, 70569 Stuttgart, (Germany)

**Departamento Física de la Materia Condensada. Universidad de Sevilla, anmube@us.es. Apdo. 1065, 41080 Seville (Spain)

***C2RMF, CNRS UMR 171, Palais du Louvre, 14 quai François Mitterrand 75001 Paris (France)

**** LEM, CNRS UMR 104, ONERA, BP 72, 92322 CHATILLON Cedex (France)

Keywords: dislocations, dissociation, decomposition, sapphire, work hardening

ABSTRACT

The properties of sapphire (α-Al_2O_3) predeformed at T = 1450 ºC by $<10\bar{1}0>\{1\bar{2}10\}$ prism plane slip and subsequently deformed in $<1\bar{2}10>(0001)$ basal slip between 1050 ºC and 1250 ºC were investigated. The critical resolved shear stress in basal slip was increased with respect to the non pre-deformed samples by a temperature-independent increment of $\Delta\tau$ = 43.6 MPa consistent with a forest dislocation mechanism. The deformation microstructures were investigated by transmission electron microscopy. Prism plane slip involves $<10\bar{1}0>$ dislocations that are essentially decomposed into two $1/3<1\bar{2}10>$ dislocations separated by a constant distance of 10 nm. No evidence of the

dissociation into three partials could be found. Reactions between dislocations of the most favored P slip system $(1\bar{2}10)[\bar{1}010]$, and of the other two less preferred P systems were frequently observed forming dipoles and junctions at moderate and high temperatures, respectively. The samples subsequently deformed in basal slip exhibit junction reactions between dislocations of the two systems. The predeformation tests were designed to engender $1/3<10\bar{1}0>$ partial dislocations presumed to be at the origin of basal twinning but no basal twins were observed.

1. INTRODUCTION

Small concentrations of dopant generally oppose dislocation glide with a strength that depends on differences in atomic radii or valences. This effect is at the origin of ~~the~~ crystal hardening, as for sapphire (α-Al_2O_3) doped with Fe, Ni, Cr or Ti [1, 2]. Cr and Ti indeed generate a hardening well accounted for by established models [2], but Mg results in a softening [3]. Doping can induce a strong coloration (e.g. Cr in ruby) whereas, next to its hardness, the transparency of sapphire from infra-red to ultraviolet is a pivotal property in many applications. In contrast, the introduction of dislocations constitutes an alternative hardening procedure with limited influence, if any, on optical properties (colour, absorption, etc). So far, the hardening of rhombohedral twinning in sapphire has been successfully achieved by basal dislocations [4].

The present work was initiated to investigate the effects of a network of $<10\bar{1}0>$ dislocations in prism planes (referred to hereafter as P dislocations) on deformation at 1050-1250°C either by slip in the basal plane (hereafter named B) or by basal twinning which has been reported once [5]. The analysis of mechanical properties is complemented by an extensive investigation of the dislocation structure after P slip, in

particular of the transformation of $<10\bar{1}0>$ P dislocations either by decomposition into perfect B dislocations or by dissociation into partials.

2. EXPERIMENTAL PROCEDURE

Sapphire (α-Al_2O_3) belongs to the $R\bar{3}c$ space group. It can be accounted for by a rhombohedral primitive cell containing two Al_2O_3 units, with lattice parameters a = 0.512 nm and α = 55º 17′ but it is usually described as a hexagonal cell with a = 0.475 nm and c = 1.297 nm. Further structural information can be found in [4, 6, 7].

2.1. Materials

Al_2O_3 single crystals grown by the Verneuil technique were provided by R. S. A. Le Rubis (Jarrie, France) under the form of cylinders approximately 3.5 cm in diameter. Impurity concentrations of Cr, Ti, Ni, Cu, Fe and Ga below 10 mol ppm were determined by PIXE (particle induced X-ray emission) at CNA (Seville-Spain) and C2RMF-CNRS (Paris-France). This material was also used in our previous works [4, 8, 9].

2.2. Sample preparation and P slip deformation

The crystals were oriented by Laue back reflection such that the compression axis lies in the basal plane half way between the $[\bar{1}\,\bar{1}\,20]$ and $[0\bar{1}10]$ directions. Among the three possible P slip systems, $(1\bar{2}10)[10\bar{1}0]$ is favored with a Schmid factor of 0.5 while the other two have a Schmid factor of 0.25. Parallelepipeds approximately 7.5 mm x 7.5 mm x 20 mm were cut with a low-speed diamond saw. The specimens were given a final polish with a diamond paste less than 3 μm in grain size for slip trace analysis by optical microscopy. The compression samples were actually too large to be encapsulated for automatic polishing without generating cracks and had to be polished manually. The load was transmitted to the specimens via SiC rods. The compression tests were performed in

an Instron machine (model 1185) at T = 1450°C in air at a constant cross-head speed of 5 μm/min corresponding to an initial engineering strain rate of $\dot{\varepsilon} \approx 4.2 \times 10^{-6}$ s^{-1}, about three times smaller than the lowest rate used by Cadoz *et al.* [10] and larger than that used by Bilde Sorensen *et al.* [11].

The samples were predeformed plastically in P slip at 1450°C until 2.5% to an applied stress of 315 MPa, necessitating rather large applied loads (~17.7 KN). In order to facilitate lubrication, the sample contact surfaces were polished and Pt foils about 0.25 mm in thickness were inserted between the sample and the pushing rods, yet the formation of cracks at the sample extremities could not be entirely eliminated.

2.3. Sample preparation and B slip deformation

Smaller parallelepiped specimens about 2.5 mm x 2.5 mm x 5.0 mm in size were prepared for deformation by B slip. For this aim, the pre-deformed samples were first sliced parallel to the P slip plane, with a thickness slightly superior to 2.5 mm (Figure 1 left). The slices were subsequently cut into deformation specimens with a compression axis at 57º from [0001] and with two lateral faces parallel to $(1\,\bar{2}\,10)$ (Figure 1 right). This orientation, dubbed *aa* [9], favors the $1/3[11\bar{2}0]$ and $1/3[2\bar{1}\bar{1}0]$ basal dislocations with a Schmid factor of about 0.4, and hampers rhombohedral twinning at intermediate temperatures.

The compression tests were performed at temperatures between 1050 and 1250 ºC at a constant cross-head speed of 5 μm/min, corresponding in this case to an initial strain rate of $\dot{\varepsilon} \approx 1.7 \times 10^{-5}$ s^{-1}.

2.4. Transmission electron microscopy (TEM).

Thin foils were prepared with a normal parallel to the $[1\,\bar{2}\,10]$, [0001] and $[2\,\bar{2}\,01]$ directions from the samples predeformed by P slip as well as from those further deformed

by B slip. The foils were mechanically ground to a thickness of about 100 μm and polished with diamond pastes with grain sizes decreased down to 3 μm. They were subsequently dimpled to ~30 μm in thickness (Dimpler grinder Gatan Model-656) and ion-beam thinned to electron transparency (PIPS Gatan Model-691) operating at 5 kV with an incidence angle decreased gradually from 10º to 4º at which angle the operating voltage was set to 4 kV in order to minimize damage. A thin carbon coating was deposited on the foils by vacuum evaporation to prevent charge build-up during the observations. The dislocation fine structure was examined under weak-beam TEM with a Jeol 200 CX electron microscope (Laboratoire d'Etude des Microstructures, CNRS-ONERA, France) and a Hitachi H-800 (CITIUS, Spain), both operating at 200 kV. Imaging plates [12] were used to record most images because the exposure times could then be considerably decreased (from 30 sec for films to 1-2 sec in weak beam) thus reducing problems associated with sample drifting.

3. RESULTS AND DISCUSSION

3.1. Deformation by P slip

The energy per unit length of a P dislocation is approximately three times larger than that of a B dislocation [6]. Both of these are potentially glissile in two distinct prism planes, i.e. $\{11\bar{2}0\}$ and $\{10\bar{1}0\}$ respectively, each perpendicular to the basal plane, but only the operation of P dislocations has been observed [11, 6, 10, 13, 14] indicating a strong lattice resistance to the motion of B dislocations in $\{10\bar{1}0\}$ planes from 1800°C down to relatively low temperatures (200-800°C) [15]. The preference for P slip is further encouraged by the possibilities that P dislocations have to refine their core structure, hence the total configurational energy. First, they can *decompose* in two B dislocations according to the reaction

$$<10\bar{1}0> \rightarrow 1/3<2\bar{1}\bar{1}0> + 1/3<11\bar{2}0> \quad (1)$$

that has been observed in P slip deformed samples forming three-dimensional networks of 1/3<2$\bar{1}\bar{1}$0> dislocations at large strains [10, 13, 14]. Second, they may dissociate into three collinear partials bordering a stacking fault in the cation sublattice with a relatively small energy (~ 0.25 J/m², the separation between partials amounts to 8-13 nm), following the reaction [6, 11, 16]

$$<10\bar{1}0> \rightarrow 1/3<10\bar{1}0> + 1/3<10\bar{1}0> + 1/3<10\bar{1}0> \quad (2)$$

According to Bilde-Sorensen *et al.* [11], the <10$\bar{1}$0> dislocation is glide-dissociated in the P plane but other observations indicate that the fault plane lies at 20° from the Burgers vector [16]. Widely climb-dissociated dislocations were also reported [16, 17].

The energy gains resulting from reactions (1) and (2) were found to be comparable [16], but this result relies on simplified calculations neglecting the elastic interaction between B dislocations. A more accurate calculation of the energies of a perfect P dislocation and of the product dislocations of reactions (1) and (2) is presented in the appendix. For comparable separations between the product dislocations, the gain associated with reaction (1) is 12% and 21% or 33% for glide and climb dissociation in reaction (2), respectively. For distances larger than 1 μm between B dislocations, reaction (1) is energetically more favorable than reaction (2). The two families of P and B dislocations are actually encountered in samples deformed in P slip. Yet, P dislocations seem to predominate at small strains [10, 13] which is the experimental condition chosen here to create the network of <10$\bar{1}$0> dislocations prior to straining in B slip.

3.1.1. Compression tests

The plastic behaviour shown in figure 2 is similar to that previously observed [10, 14]. The flow stress is however somewhat higher which can be ascribed to the

dependence of the flow stress on sample geometry [18-19]. In order to retain the dislocation structure generated during deformation (2.5% of strain under an applied stress of 315 MPa at 1450°C) and, in particular to hinder reaction (1) expected to occur at high temperature once dislocations have stopped, sample cooling was carried out under 310 MPa down to 1300ºC, then 290 MPa between 1300 and 1200ºC, 200 MPa between 1200 and 1050ºC, below which the stress was released since then the dislocations are expected to be frozen by lattice friction. Slip line analysis by optical microscopy confirmed that $(1\bar{2}10)[\bar{1}010]$ was the main slip system activated.

3.1.2. Dislocation structure

Figure 3 is a representative TEM view of a foil cut parallel to the slip plane that contains typical features such as perfect and faulted loops (PL, FL) and long curved P dislocations. Reactions (R) between dislocations $\mathbf{b_1} = [\bar{1}010]$ of the most favored P slip system $(1\bar{2}10)[\bar{1}010]$, and $\mathbf{b_2} = [\bar{1}100]$ or $\mathbf{b_3} = [01\bar{1}0]$ of the other two less preferred P systems were frequently observed. Dislocation curvatures such as in figures 3 and 4, provide an estimate of local stresses via the expression:

$$\tau = \frac{\alpha \mu b}{r} \qquad (3)$$

where r is the radius of curvature, α is a constant between 0.3 and 0.5, μ is the shear modulus (156 GPa) and b is the norm of the Burgers vector (0.822 nm). The local stress varies between 130 and 340 MPa indicating that lattice friction is of the order of the stresses applied at the end of the mechanical test and during the cooling (§ 3.1.1 and figure 2).

In figure 3, some junctions marked R result from the reaction of two of the P dislocations yielding the third one. The dislocation with Burgers vector $\mathbf{b_1}$ displays a decomposition process (e.g. D) via reaction (1) into two basal dislocations $1/3[\bar{2}110]$ and $1/3[\bar{1}\,\bar{1}20]$ as shown in the insets (ii) and (iii). The portions where the dislocation

exhibits a single/double line are interchanged upon reversing the sign of the offset from Bragg condition, $s_{\mathbf{g}}$. This property results from a dipolar contribution to the image and reflects the fact that at some point along basal dislocations exchange their positions in projection. In the lower nearly vertical portion of feature D in figure 3, the transition from a single to a double line occurs exactly in the screw orientation while in a non-screw orientation in figure 4. In figure 3 the property that the decomposition into two basal dislocations is not visible for dislocations with Burgers vectors $\mathbf{b}_2 = [\bar{1}100]$ and $\mathbf{b}_3 = [01\bar{1}0]$ stems from the fact that one of the by-products, the partial with Burgers vector $1/3[\bar{1}2\bar{1}0]$, is invisible under $\mathbf{g} = \bar{3}030$. The decomposition, which in figure 3 is viewed in the primary glide plane, is of the same kind as that reported by Cadoz *et al.* (figure 7 in [10]). In polycrystalline alumina deformed under wet hydrostatic pressure at 700°C, pairs of B dislocations were observed along the [0001] direction (figure 12 in [20]). The faulted (FL) loops are dissociated in two or three partial dislocations, in consistency with previous observations [17]. By means of a specific stereographic method [21], we have determined that the loop is faulted approximately normal to the slip plane $(1\bar{2}10)$ indicating that dissociation has taken place essentially by climb, again in agreement with [17]. The precision of such a determination is, however, rather poor (±15°). It cannot be ascertained that the dissociation plane is strictly perpendicular to the loop habit plane hence a possible contribution of glide in the dissociation process.

Dislocation junctions are generated along the [0001] direction cozonal with the three prismatic planes by the reaction of two P slip dislocations. Provided such junctions remain in place during deformation, the configuration then allows distinguishing between the reacting dislocations and their end-products. In figure 4, dislocations $\mathbf{b}_2$ and $\mathbf{b}_3$ indeed generate the junction $\mathbf{b}_1$ oriented along the [0001] direction that itself exhibits a double line over half of its length and a single, thicker one elsewhere. As already observed in figure 3, the situation is reversed upon changing the sense of $s_{\mathbf{g}}$ (inset). The observation is

consistent with the junction initially edge in character with Burgers vector $\mathbf{b_1}$ having decomposed into two repulsive B dislocations according to reaction (1). Each decomposition by-product is potentially glissile in a distinct $\{1\bar{1}00\}$ plane. As for the similar examples shown in figure 3, the fact that their separation remains moderate (about 10 nm in projection) attests to a very high friction stress experienced by B dislocations out of the basal plane. Similar observations have been made in polycrystals deformed under hydrostatic pressure at low temperatures [20]. It is worth emphasizing that the junction's Burgers vector, $\mathbf{b}_1$, determined in figure 4 coincides with the most stressed slip direction and thus results from the reaction of two lesser stressed slip directions. This paradoxical situation does not actually stem from some arbitrary choice made on orientation conventions upon indexing the thin foil since this foil was cut to parallel to the $(1\bar{2}10)$ operative P plane which contains only one $<\bar{1}010>$ direction, the $\mathbf{b_1}$ = $[\bar{1}010]$, slip direction. It must therefore be concluded that dislocations $\mathbf{b}_2$ and $\mathbf{b}_3$ could slip over some distance after they were generated, in spite of relatively unfavorable Schmid factors (0.25), and that this motion did not involve climb since the junction is well aligned with the [0001] direction.

Besides being decomposed, we expect finding P dislocations dissociated into three partials (reaction (2), section 3.1). Should the dissociation plane lie at 20° to the glide plane as previously reported [16], observing such dissociation is in principle straightforward in foils parallel to the prism slip plane (figures 3 and 4) but no such configuration was detected in the present investigation. The only dissociation process of P dislocations which we have identified in the pre-deformed samples occurred at the already mentioned loops (see above) as well as along a segment length of about 40 nm (not shown here) lying in a secondary slip plane at 60° from the primary slip plane, thus at variance with previous investigations that have reported long dissociated P dislocations [11, 22, 23]. Bilde-Sorensen *et al.* [11] analyzed specimens deformed in bending at a

temperature unfortunately not documented. Since they were taken from a series of experiments achieved by Gooch and Groves [24] where P slip was activated down to 1100°C, it is plausible that the glide dissociation of P dislocations reported by Bilde-Sorensen *et al.* [11] was observed in samples deformed at the lowest temperatures. Various $<10\bar{1}0>$ dislocations were reported exhibiting single, double and triple contrast. The single contrast was ascribed to perfect dislocations and the triple contrast to three $1/3<10\bar{1}0>$ partial dislocations split apart by glide (the foil was cut in the glide plane). Still lower temperatures were tested by Farber *et al.* [22] and Cadoz *et al.* [23] who activated P slip by indentation below 1000°C and under a hydrostatic pressure of 1500 MPa at 400°C, respectively. It is worth noting that the above-mentioned observation of a threefold 20° off-glide dissociation [16] was conducted in specimens deformed at a relatively high temperature of 1450°C but air-quenched (pulled out of the furnace) to hamper post deformation dislocation relaxation. The present experimental conditions (figure 2) have not allowed observing glide dissociated P dislocations.

The exact fine structure of gliding P dislocations is not yet clearly identified. According to the TEM observations, they may be perfect $<10\bar{1}0>$ P dislocations, pairs of perfect $1/3<1\bar{2}10>$ B dislocations, or else threefold P dislocations glide dissociated into collinear $1/3<\bar{1}010>$ partials. It is not expected that the same dislocation structure prevails in the whole range of deformation temperatures, i.e. from 200°C and 1800°C, that has been explored so far [25]. Unambiguous observations of glide dissociation are rare compared to those of climb dissociation. For an edge P dislocation, the gain in energy for the latter core configuration amount to 10 % of the energy of the former (see appendix). At high enough temperature for the exchange point defects between partials to take place, it is plausible that climb dissociation occurred after glide dissociated dislocations have stopped their motion. The occurrence of climb-dissociated P dislocation [10, 17] after high temperature deformation (T>1450°C) is compatible with the

dominating presence of the usual 1/3<1 $\bar{2}$10> climb-dissociated B dislocations [6, 21]. The latter which results from reaction (1), provides a further gain in energy when B dislocations are far apart (see the appendix). At high temperature, the decomposition of a climb-dissociated P dislocation into two climb-decomposed B dislocations has been observed by TEM with no constriction at the node [16] showing that there is no obstacle for reaction (1) to take place. The decomposition mechanism (reaction 1) explains why only B dislocations are observed after large deformation by P slip above 1400-1450°C [10] as climb allows B dislocations to move apart over long distances (several micrometers) to form a 3-dimensional network at large strains [10].

In order to bring new arguments into the understanding of the dislocation mechanisms involved in P slip, we have performed a detailed calculation of the elastic energies of the four possible P dislocation configurations, viz. perfect, glide dissociated, climb dissociated and decomposed in two B dislocations at short and long distances (see details in the appendix). One of the most important issues is concerned with the origin of P dislocation sources. Obviously, perfect P dislocations should not exist in as-grown sapphire since reaction (1) provides a large energy gain when the two B dislocations are 1 µm apart (see appendix). This is actually confirmed by a number of X-ray topography observations where only Burgers vectors parallel to <1 $\bar{2}$10> have been identified [26-29] but for one investigation [30]. Further to relatively rare segments [30], P dislocations may exist in the subsurface layer where a few short segments (less than 130 nm) have been observed and ascribed to the mechanical polishing of a $\{11\bar{2}0\}$ face of sapphire with 1 µm diamond slurry [31]. Should very short P segments exist as perfect dislocations, they could be at the origin of perfect P dislocation sources activated under large stresses, that is, at low temperature. Such P dislocations are prone to dissociating (reaction 2) by glide as this results in an energy gain of about 20 % (appendix) and is observed by TEM [22, 23] after P slip deformation at low temperature. Alternatively, at intermediate and high

temperatures, P dislocations are likely to be formed upon the crossing of two B dislocations and to subsequently expand in a P plane when in the screw orientation. Depending on the conditions of deformation, such P dislocations may dissociate into three partials by climb when temperature and dynamics allow (33 % energy gain; appendix) or decompose back in two B dislocations. At intermediate temperatures (900-1100°C), B dislocations are paired and separated on average by approximately 10 nm that corresponds to an energy gain of about 12%. This distance reflects the balance between the repulsion stress (about 500 MPa [20]) and the friction stress in each dislocation's respective $\{1\,\bar{1}\,00\}$ glide planes, consistent with the features observed in figures 3 and 4.

In brief, energy considerations suggest that in sapphire P dislocations should be glissile at low temperatures while at high temperature they should decompose into correlated pairs of B dislocations. This view is actually supported by TEM observations [10, 11, 15, 22, 23] together with the observation that compared to B slip P slip is easier below 700°C and more difficult at high temperature [15, 36]. This suggests in turn that the mobility of P dislocations is ~~relatively~~ large relative to B slip at low temperature. Careful examination of the crystal structure brings no elements suggesting that $1/3<10\,\bar{1}\,0>$ partials are submitted to a strong lattice friction in $\{1\,\bar{2}\,10\}$ planes [6]. The decrease of P dislocation mobility above 700°C is consistent with their core extension out of the P slip plane via either reaction (1) or (2). Further work is necessary to check these conclusions.

3.2. Deformation of aa samples in basal slip

$1/3<11\bar{2}0>(0001)$ B slip is the easiest deformation mode of sapphire (α-Al_2O_3) above its brittle to ductile transition temperature which, in standard mechanical tests, amounts to about 900°C [32]. B dislocations do not dissociate by glide since the stacking

fault in the basal plane is prohibitively large [6] but by climb in two partial dislocations [6, 16, 21] following

$$1/3<11\bar{2}0>\rightarrow 1/3<10\bar{1}0>+1/3<01\bar{1}0> \quad (4)$$

As for the dissociation of a P dislocation, the stacking fault only affects the cation sublattice.

3.2.1. Latent hardening of basal slip

The stress-strain curves of samples predeformed in P slip and subsequently compressed in the *aa* direction between 1050 and 1250 ºC shown in figure 5 strongly remind of *aa* sapphire samples deformed directly by basal slip [9]. The lower yield point is followed by a domain of still increasing stress. Here the work-hardening rate is about μ/20 - μ/30 between 1250°C ~~to~~ and 1050°C, higher than the μ/50 as for non predeformed samples [33]. In the samples deformed at the highest temperatures, the upper yield point is hardly noticeable (figure 5). It is worth emphasizing that stress drops that would have attested to twinning were never observed.

The temperature dependence of the critical resolved shear stress (CRSS) measured at the lower yield point is shown in figure 6. Comparison with previous results [9, 34] reveals that the hardening is stronger in the presence of P dislocations (latent hardening) than as a result of Cr additions, even for dopant concentrations as high as 9540 mol ppm [34]. An appreciation of the difference in strength of the two types of obstacles is provided by their distribution in the lattice, every 1.3 nm for the of 9540 mol ppm Cr compared to an average of approximately 1 μm between the P dislocations of the forest (dislocation density $\rho \sim 10^{12}$ m^{-2}). Latent hardening is athermal in the temperature range investigated (figure 6). After pre-deformation, the resolved shear stress (RSS) in the basal plane ~~is~~ can be analyzed as the sum of two terms:

$$\tau = \tau_0 + \Delta\tau \tag{5}$$

where τ_0 is the RSS of a non pre-deformed sample and $\Delta\tau$ the temperature independent additional RSS required to destroy junctions with the forest dislocations, given by [35]:

$$\Delta\tau = \alpha\mu b\rho_p^{1/2} \tag{6}$$

In a previous work [36], the temperature dependence of the CRSS in basal slip was shown to be consistent with the kink-pair model in the long-segment limit provided this model is corrected for the stress dependence of the dislocation density. The model is represented by the lower solid line in figure 6. With the same set of parameters as in [36] and substituting $\tau_0 = \tau - \Delta\tau$ for the applied shear stress, one obtains the upper solid line in figure 6 which for $\Delta\tau$ = 43.6 MPa is in excellent agreement with experimental data. This substitution thus assumes that the driving force to nucleate and move kinks is the applied shear stress minus the average stress used to overcome the interaction between the primary B dislocations and the forest P dislocations. With α = 0.5, μ = 156 GPa, b = 0.475 nm and $\Delta\tau$ = 43.6 MPa, Eq. (6) yields a forest density of $\rho_p = 1.4\cdot10^{12}$ m^{-2} which, as far orders of magnitude are concerned, is consistent with ~~an~~ the average density of about $5\cdot10^{12}$ m^{-2} measured by TEM (ratio between the total length of the dislocations in the foil and the foil volume) in the pre-deformed samples. Alternatively, the dislocation density at the end of the pre-deformation stage can be also calculated with the expression

$$\rho = \left(\frac{\tau}{C\mu b}\right)^2 \tag{7}$$

used by Castillo *et al.* [36] to account for its dependence on the CRSS in P slip at the lower yield point. Taking C = 2.8 [36] and from the experimental data of Cadoz *et al.* [10] (τ = 99 MPa under a strain rate of $\dot{\varepsilon} = 1\cdot10^{-5}$ s^{-1} at T = 1450 ºC), the kink pair model yields $\rho_p = 2.3\cdot10^{11}$ m^{-2}, again fairly consistent with the above model-fitted and

experimental values.

3.2.2. The microstructure in samples deformed by basal slip

An example of the dislocation microstructure in samples-subsequently strained by B slip at 1200 °C is shown in figure 7. The foil, cut parallel to the primary P slip system, exhibits perfect and faulted loops (PL, FL) as well as reactions (R) between prismatic dislocations generated during pre-deformation and elongated in the [0001] direction. After reaction, the resulting prismatic dislocation can decompose in two B dislocations (short horizontal arrow, D in inset). The dipolar character of one of these is demonstrated by comparison with the left inset of figure 7, taken under s_g <0 and s_g >0, respectively. By tilting by 10° about the $[\bar{1}\bar{1}26]$ direction from the $[\bar{2}4\bar{2}1]$ zone axis, which lies at ~ 30° from the primary P slip plane (upper right inset), one sees that the features labeled 1-8 remain normal to the [0001] direction, increasing their length though but showing no evidence of them being loops. Hence, since no double or triple contrast is observed upon reversing the sign of $s_{\mathbf{g}}$, they are basal dislocations generated by the second deformation whose lines are almost perpendicular to the foil. They are in contrast under $\mathbf{g} = 10\bar{1}4$ thus ruling out $\mathbf{b} = 1/3[\bar{1}2\bar{1}0]$ and leaving either $\mathbf{b} = 1/3[11\bar{2}0]$ and $\mathbf{b} = 1/3[2\bar{1}\bar{1}0]$ both equally activated under the compression axis selected here (section 2.3). It is noted that dislocation 8 is stopped by ~~has impacted~~ at the long pair of B dislocations. Additional configurations similarly involving reactions between B and P dislocations are observed in figure 8. In the center of the micrograph, two P dislocations 1-1' ($\mathbf{b}_{1\text{-}1'} = [10\bar{1}0]$) react with 2-2' ($\mathbf{b}_{2\text{-}2'} = [0\bar{1}10]$) forming 3 ($\mathbf{b}_3 = [1\bar{1}00]$). It is worth emphasizing that the latter is not oriented along [0001] thus attesting to a significant rearrangement by climb. The configuration on the right-hand side of figure 8 is comprised of two P dislocations ($\mathbf{b}_4 = [\bar{1}010]$ and $\mathbf{b}_5 = [10\bar{1}0]$) and three basal dislocations with $\mathbf{b}_{6\text{-}8} = 1/3[\bar{1}\bar{1}20]$ (6 and 8, with segment 8 very short thus hardly visible) and $\mathbf{b}_7 = 1/3[2\bar{1}\bar{1}0]$ (7). It is emphasized that in

its upper part, the image of dislocation 4 splits into two as was observed in figures 3, 4 and 7. The whole configuration is consistent with the property (figure 8b) that the B dislocation 6-8 has ~~impacted~~ reacted differently with the two branches of the P dipole producing no junction with 4 because the segment with b= $1/3[\bar{4}\,\bar{1}\,50]$would be that is energetically unfavorable. By contrast, the reaction with dislocation 5 yield the junction 7 according to:

$$[10\bar{1}0] + 1/3[\bar{1}\,\bar{1}20] \rightarrow 1/3[2\bar{1}\,\bar{1}0] \qquad (8)$$

Similar reactions now more conspicuous are found in foils cut parallel to the B ~~slip~~ plane (figure 9) hence confirming that the hardening of B slip stems from the forest P dislocations (§ 3.2.1). The dislocation structure in the present specimens is significantly different from that encountered in samples doped with Cr and strained under similar conditions [23]. Doping with Cr hardly modifies dislocation microstructure and its effect is reduced to an increase of the Peierls barriers due to the differences in elastic modulii and sizes arising from substitutional Cr [28] and a small decrease in the SFE of B dissociated dislocations [21]. However, a predeformation by P slip has a strong influence on B dislocation due to the high amount of reactions bewteen B and P dislocation forest, leading to the latent hardening observed in figure 6**.**

The interaction between a P forest dislocation and a B dislocation differs considerably depending whether the reaction is energetically favorable or not. In case it is unfavorable, the two dislocations cross through one another engendering kinks in the direction of the Burgers vector of the other dislocation. The energy barrier associated with this process may prevent the B dislocation from cutting through (e.g. feature 8 in figure 7). Since the two Burgers vectors belong to the B plane, the kinks disappear by glide as the dislocation slips forward. In case the reaction is favorable, junctions are generated as shown in figure 9 where, for example, in the up left inset a $1/3[11\bar{2}0]$ B_1

dislocation reacts with a $[\bar{1}010]$ P dislocation to give a $1/3[\bar{2}110]$ B_2 dislocation. As expected the junctions, pointed by arrows, are located at the intersection between the basal plane and the $(1\bar{2}10)$ plane where the pre-deformation was activated. It is worth emphasizing that segment B1, which is imposed by the rule of Burgers vector conservation, is invisible under all g-vectors tested, indicating that this portion of the configuration is very close to the surface. Due to the large friction opposing the glide of P dislocations in the basal plane and of basal dislocations out of the basal plane, such junctions cannot lengthen without the assistance of atom transport. They impede the glide of B dislocations and are responsible of the relatively strong hardening observed in the present compression tests.

3.2.3 Basal twinning

He *et al.* [37] have found by weak-beam TEM that P dislocations with a $[10\bar{1}0]$ Burgers vector dissociate into three $1/3[10\bar{1}0]$ partial dislocations located at the interface between a twin and the matrix. This observation and a few others [38] have been regarded as a confirmation of the operation of the basal twinning mechanism in sapphire given in [6, 39, 40]. According to this model, the glide of a partial $1/3[10\bar{1}0]$ dislocation in the basal plane generates a stacking fault with local twin symmetry. The partial dislocations can recombine into a perfect P dislocation which, if screw in character, can ascend to an adjacent basal plane by cross-slip and generate a partial dislocation in this plane creating a micro-twin. The repetition of this process results in a basal twin [6, 39, 40].

In the present investigation, no micro-twins could be observed by TEM. The presence of a significant density of $<10\bar{1}0>$ P dislocations capable of dissociating into three collinear $1/3<10\bar{1}0>$ partial dislocations could have provided many sources for

micro-twins but no such dissociated dislocation has been identified in samples pre-deformed at 1450ºC. Instead, P dislocations appear most of the time as pairs of B dislocations resulting from reaction (1). The dissociation of P dislocations into three $1/3<10\bar{1}0>$ partials is actually absent in sapphire deformed in P slip except in the above-mentioned faulted loops which are however too small to give rise to this mechanism. Macroscopically, there is no indication of twinning on stress-strain curves (figure 5) and twins are detected by optical microscopy neither in reflection nor in transmission. The present investigation thus provides essentially negative conclusions regarding the operation of basal twinning in sapphire as regards the model recently proposed by Lagerlof *et al.* [38]. It does not help either to understand the conditions that prevailed in the experiments of Conrad et al. [5] who reported the activation of basal twinning under normal compression tests of sapphire at 1200°C and 1500°C.

4. CONCLUSIONS

- Compression tests conducted between 1050 ºC and 1250 ºC show that the presence of P dislocations in sapphire generated by a pre-deformation at T = 1450 ºC results in a significant hardening of basal slip. The effect is athermal and is more potent than doping with Cr even under high concentrations (9540 mol ppm).
- P dislocations undergo decomposition into two basal dislocations whose small separation attests to a low mobility of the latter off the basal plane. On the other hand, dissociation into three partials is seldom observed.
- The forest dislocation model provides an explanation to the observed work-hardening of basal slip whose rate (μ/20-μ/30) is about twice that measured in non pre-deformed P slip samples (μ/50). Basal dislocations interact with the forest of P dislocations producing junctions with basal dislocations that hinder the glide of the latter.

- The resulting increment of the critical resolved shear stress is $\Delta\tau$ = 43.6 MPa, in good agreement with two independent evaluations of the densities of P forest dislocation densities.
- The activation of basal twining has not been observed.

Acknowledgements

This work has been supported by the Ministry of Science and Technology (Government of Spain) through the "Proyecto Excelencia JA P05-03337-FQM".

REFERENCES

[1] Radford KC, Pratt PL. Proc Brit Ceram Soc 1970;15:185

[2] Pletka BJ, Mitchell TE, Heuer AH. Phys Stat Sol, (a) 1977; 39:301

[3] Lagerlof K P D, Pletka B J, Mitchell T E, Heuer A H. Radiation Effects 1983; 74:87

[4] Castaing J, Muñoz A, Dominguez Rodríguez A. Philos Mag A 2002; 82: 1419

[5] Conrad H, Janowski K, Stofel E. Trans Metall Soc AIM 1965;223:255

[6] Heuer AH, Lagerlöf KPD, Castaing J. Philos Mag A 1998;78**:**747

[7] Bilden-Sørensen JB, Lawlor BF, Geipel T, Pirouz P, Heuer AH, Lagerlöf KPD. Acta Metall Mater 1996;44:2145

[8] Castaing J, He A, Lagerlöf KPD, Heuer AH. Philos Mag A 2004;84:1113

[9] Castaing J, Muñoz A, Gómez García D, Domínguez Rodríguez A. Mater Sc Eng A 1997;233:121

[10] Cadoz J, Castaing J, Phillips D S, Heuer A H, Mitchell T E. Acta Metall, 1982;30**:**2205

[11] Bilden-Sørensen JB, Thölen AR, Gooch DJ, Groves GW. Philos Mag 1976;33:877

[12] Zuo JM. Microscopy Research and Technique 2000;49:245

[13] Cadoz J, Hokim D, Meyer M, Rivière J P. Rev Phys Appl 1977;12:473

[14] Kotchick D M, Tressler R E, J Amer Ceram Soc 1980;63:429

[15] Lagerlöf KPD, Heuer AH, Castaing J, Rivière J-P, Mitchell TE. J Amer Ceram Soc 1994;77:385

[16] Lagerlöf KPD, Mitchell TE, Heuer AH, Rivière JP, Cadoz J, Castaing J, Phillips D. Acta Mettall. 1984;32**:**97

[17] Phillips D, Cadoz J. Philos Mag A 1982;46**:**583

[18] Bretheau T, Castaing J, Veyssiere P, Rabier J. Adv Phys 1979;28:835

[19] Rivière J P, Castaing J. J Amer Ceram Soc 1997;80:1711

[20] Lartigue S, Castaing J. J Amer Ceram Soc 2003;86:566

[21] Castillo Rodríguez M, Castaing J, Muñoz A, Veyssière P, Domínguez Rodríguez A. Acta Mater 2009;57:2879

[22] Farber Ya, Yoon SY, Lagerlöf KPD, Heuer AH. Phys Stat Sol (a) 1993;137:485

[23] Cadoz J, Rivière JP, Castaing J, Deformation of Ceramics II , edited by Tressler R.E., Bradt R.C., Plenum Publishing corporation 1984, p. 213

[24] Gooch DJ, Groves GW. Philos Mag 1973;28:623

[25] Castaing J, Cadoz J, Kirby SH. J Amer Ceram Soc 1981;64:504

[26] Caslavsky JL, Gazzara CP, Middleton RM. Philos Mag, 1972;25:35

[27] Caslavsky JL, Gazzara CP. Philos Mag 1972;26:961

[28] Wada K., Hoshikawa K. J Cryst Growth 1980;50:151

[29] Qiang Z, Peizhzn D, Fuxi G. J Cryst Growth, 1991;108:377

[30] Takano Y, Kohn K, Kikuta S, Kohra K. Jap J Appl Phys 1970; 9:847

[31] Saito T, Hirayama T, Yamamoto T, Ikuhara Y. J Amer Ceram Soc 2005;88:2277

[32] Kim HS, Roberts S. J Amer Ceram Soc 1994;77:3099

[33] Pletka BJ, Heuer AH, Mitchell TE. Acta Met 1977;25:25

[34] Castillo Rodríguez M, Muñoz A, Castaing J, Veyssière P, Domínguez Rodríguez A. J Eur Ceram Soc 2007;27:3317

[35] Saada, G. Acta Met1960; 8:841

[36] Castillo Rodríguez M, Castaing J, Muñoz A, Veyssière P, Domínguez Rodríguez A. J Amer Ceram Soc, 2008;91**:**1612

[37] He A, Lagerlöf KPD, Castaing J, Heuer AH. Phil Mag A, 2002;82**:**2855

[38] Lagerlöf KPD, Castaing J, Pirouz P, Heuer AH. Phil Mag A 2002;82:2841

[39] Geipel T, Bilden-Sørensen JB, Lawlor BF, Pirouz P, Heuer AH, Lagerlöf KPD. Acta Metall Mater 1996;44:2165

[40] Pirouz P, Lawlor BF, Geipel T, Bilden-Sørensen JB, Lagerlöf KPD, Heuer AH. Acta Metall Mater 1996;44:2153

[41] Castaing J, Cadoz J, Kirby SH. J Physique 1981;42:C3-43

[42] Hirth JP, Lothe J. Theory of dislocations, John Wiley & Sons Ltd, 1982

[43] Mitchell TE, Heuer AH. Dislocations and mechanical properties of ceramics. Dislocations in Solids, vol 12. Amsterdam: Elsevier; 2005. p. 339

APPENDIX

Energies of the various possible sets of dislocations associated to P slip

$<10\bar{1}0>$ P dislocations may dissociate into three collinear partials (reaction 1) or else decompose into two perfect B dislocations (reaction 2). Highly simplified calculations [16] conclude to similar energy gains whatever the reaction. More accurate calculations of the total elastic energy should help to understand which configuration, either dissociation or decomposition, is preferred.

The contributions of the self-energy w and interaction energy w_{12} per unit length are written:

$$w = \frac{\mu}{4\pi}\left(\left((b\cdot\xi)(b\cdot\xi) + \frac{(b\times\xi)\cdot(b\times\xi)}{1-\upsilon} \right) Ln\left[\frac{R_o}{R_i} \right] \right)$$

$$w_{12} = -\frac{\mu}{2\pi}\left(\left((b_1\cdot\xi)(b_2\cdot\xi) + \frac{(b_1\times\xi)\cdot(b_2\times\xi)}{1-\upsilon} \right) \left(Ln\left[\frac{r}{R_o} \right] \right) + \frac{[(b_1\times\xi)\cdot r][(b_2\times\xi)\cdot r]}{(1-\upsilon)r^2} \right)$$

respectively [42], where the inner cut-off radius R_i is ascribed the length of the Burgers vectors. For simplicity, the ratio between the outer and inner cut-off radii is kept constant ($R_o/R_i = 10^4$). We take ν = 0.24 for the Poisson ratio.

In the case of decomposition reaction (1) where two B dislocations are produced, we have considered that the decomposition plane is normal to the $\{1\bar{2}10\}$ prism plane slip, which coincides to the basal plane in the screw P dislocation. The total energy of a P dislocation decomposed in two basal dislocations can be written:

$$E_D = 2w(basal) + w_{12}$$

The energy of a P dislocation dissociated into three collinear partials, by glide or by climb, is written:

$$E_{Di} = 3w(partial) + w_{12} + w_{23} + w_{13} + 2(\gamma\cdot d)$$

where $w_{12} = w_{23}$ and the last term contains the stacking fault energy (γ = 0.25 J/m² [16]) bordered by these three partials.

Figure A-1 shows, in $\frac{\mu a^2}{2\pi}$ units ($\frac{\mu a^2}{2\pi}$ = 5.4 nJ/m, with a = 0.475 nm and μ = 156 GPa), the energy dependence on the dislocation character θ of an undissociated P dislocation (black curve) which, as expected, is the highest. The dissociation by climb (red) is more favorable than by glide (green) in agreement with the commonly observed predominance of climb dissociation in many oxides, including sapphire, whose fault energy is fairly isotropic out of the (0001) basal plane [43]. The energy difference, which is a maximum

in the edge orientation, decreases as the screw component increases. However, it is worth emphasizing that P screw dislocations cannot dissociate normal to the $\{1\bar{2}10\}$ plane since this coincides with the basal plane where the stacking fault energy is one order the magnitude higher [6, 43]. This fact has not been taken into account. We have in addition plotted the separation dependence of the energy gain of a P dislocation decomposed in two basal dislocations. Note that it is not until a separation above ~ 1 μm between basal dislocations that decomposition (reaction 1) starts to be energetically more favorable than dissociation (reaction 2).

FIGURE CAPTION

Figure 1. Samples for deformation by B slip are cut in the sample pre-deformed by P slip. Left: position of the B slip specimens inside the P slip specimen. Right: top view of a slice cut parallel to the P slip plane showing the final cut of *aa* oriented B slip specimens.

Figure 2. Stress-strain curve of a sample of sapphire deformed by P slip at T = 1450 ºC. The plastic strain amounts to about 2%. The applied stresses during the cooling are indicated for each interval of temperatures.

Figure 3. The typical microstructure of the sample strained by P slip at 1450 ºC showing faulted and unfaulted loops (FL, PL), reactions (R) between P dislocations and the decomposition process (D) of a prismatic dislocation into two parallel B dislocations about 10 nm apart. $\mathbf{b_1}=[\bar{1}010]$, $\mathbf{b_2}=[\bar{1}100]$ and $\mathbf{b_3}=[01\bar{1}0]$. The foil is parallel to the P slip plane $(1\bar{2}10)$. Inset (i) is a view under $s_g > 0$ of the configuration pointed to by an arrow, at the same magnification. Notice that the contrast has been reversed to enhance visibility. Insets (ii) and (iii) are magnification views of the same curved segment shown by an arrow; they are imaged under $s_g < 0$ and $s_g > 0$, respectively.

Figure 4. Micrographs of the specimen deformed by P slip at 1450 °C. $\mathbf{b_1}=[\bar{1}010]$, $\mathbf{b_2}=[\bar{1}100]$ and $\mathbf{b_3}=[01\bar{1}0]$. The foil is parallel to the slip plane $(1\bar{2}10)$. The view in the upper left box was taken under the opposite sign of s_g and shows the crossing between B dislocations produced after the decomposition process (D).

Figure 5. Engineering stress-strain curves of sapphire deformed by B slip at different temperatures. The samples were pre-deformed by P slip.

Figure 6. Experimental values of the CRSS vs. temperature for B slip in specimens previously deformed by P slip. The experimental values obtained by various authors [9,

41] for the B slip of sapphire without pre-deforming are included. The solid lines correspond to the fits from the kink pair model to the experimental values of the CRSS.

Figure 7. Dislocations in a sample pre-deformed by P slip at 1450 °C and by B slip at 1200°C. Reversing the sign of s_g indicates that at short distance from the reaction (R) between $[10\bar{1}0]$ and $[0\bar{1}10]$ P dislocations, the long product dislocation parallel to [0001] decomposes in two B dislocations (D, inset on the left for $s_g > 0$). B dislocations (1 to 8) are observed by tilting (up right inset)

Figure 8. (a) Reactions between B and P dislocation in a sample pre-deformed by P slip at 1450°C and then deformed by B slip at 1200°C. The reaction between a P dipole and a B dislocation is observed. The foil is normal to $[\bar{1}2\bar{1}0]$. (b) A schematic of the process yielding the configuration on the right.

Figure 9. Dislocation microstructure in a sample pre-deformed by P slip at 1450 °C and by B slip at 1100°C. The foil is parallel to the basal plane. Up left an enlarged positive print of the reaction between P and B dislocations at the node pointed by an arrow is shown (segment B_1 is not visible).

Figure A-1. Plots of the energy per unit of length dislocation E (in $\frac{\mu a^2}{2\pi}$ = 5.4 nJ/m units, with a = 0.475 nm and μ = 156 GPa) of an undissociated (black) and dissociated or decomposed P dislocations, depending on the dislocation character θ. The dissociations by glide and by climb are represented by the green and red lines, respectively (the latter is invalid in the screw orientation). The decomposition in two B dislocations is represented by the blue, cyan, orange and purple curve for a separation of 10 nm, 1 μm, 10 μm and 100 μm, respectively.

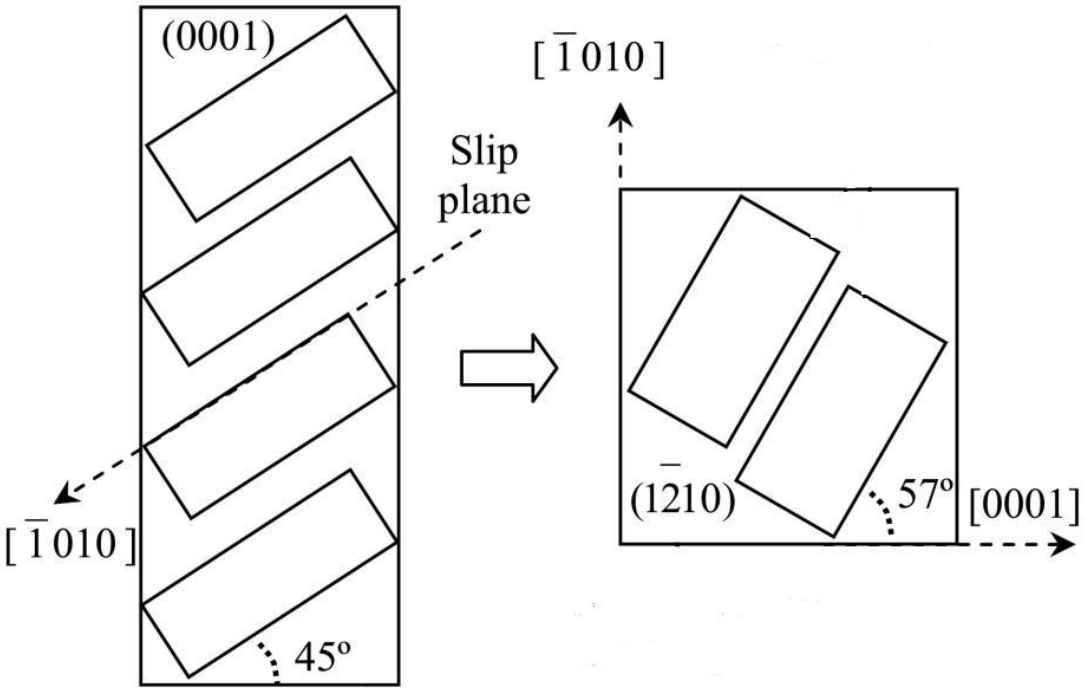

Figure 1

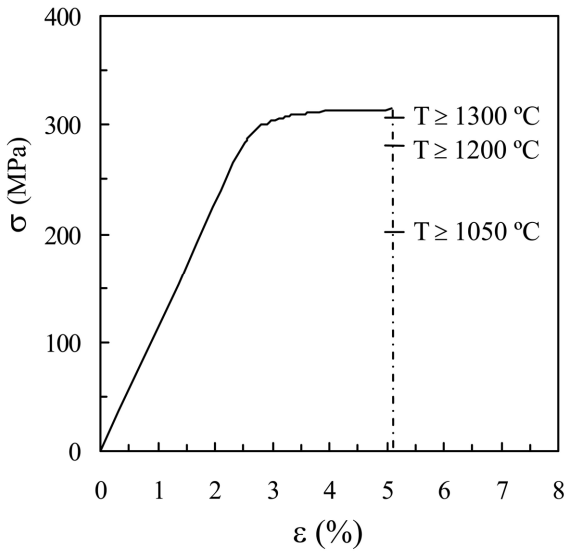

Figure 2

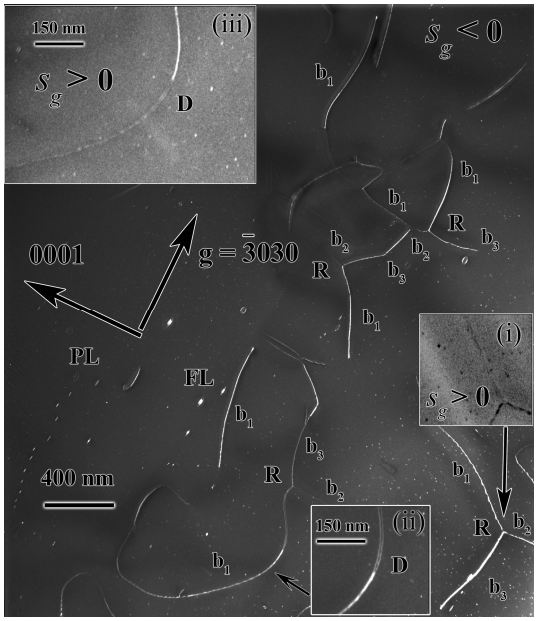
150 nm
(iii)
$s_g > 0$
D
$s_g < 0$
b_1
b_1
b_1
R
b_3
b_2
b_2
R
b_3
b_1
0001
$g = \bar{3}030$
PL
FL
(i)
$s_g > 0$
b_1
b_3
R
b_2
b_1
400 nm
150 nm
(ii)
R
b_2
D
b_1
b_3

Figure 3

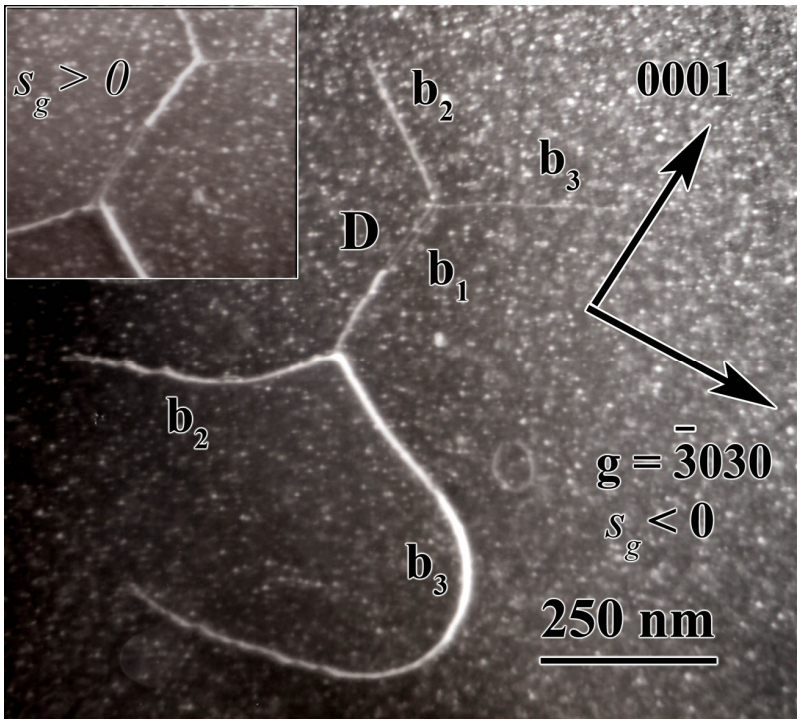
$s_g > 0$
$\mathbf{b}_2$
0001
$\mathbf{b}_3$
D
$\mathbf{b}_1$
$\mathbf{b}_2$
$\mathbf{g} = \bar{3}030$
$s_g < 0$
$\mathbf{b}_3$
250 nm

Figure 4

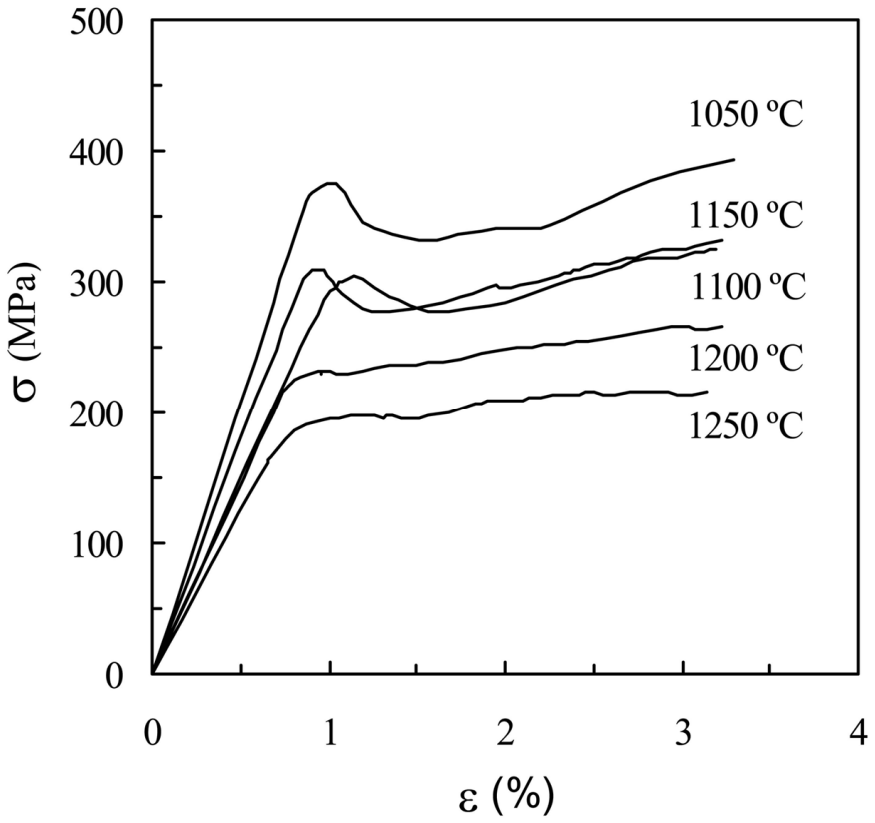
500
400
300
200
100
0
σ (MPa)
0
1
2
3
4
ε (%)
1050 ºC
1150 ºC
1100 ºC
1200 ºC
1250 ºC

Figure 5

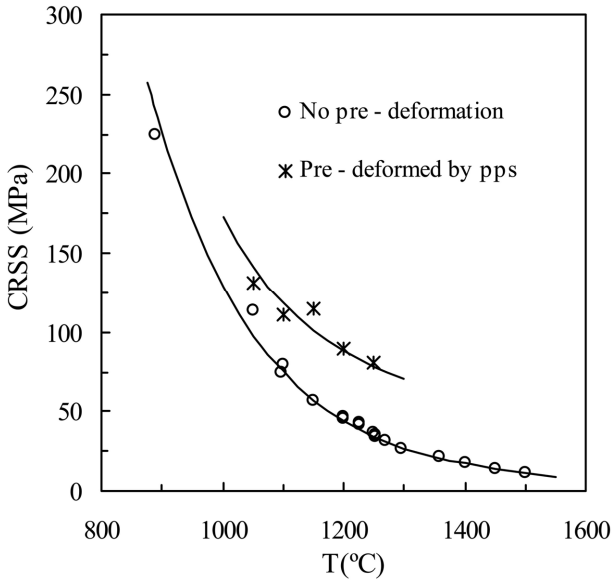
300
250
200
150
100
50
0
CRSS (MPa)
800
1000
1200
1400
1600
T(ºC)
No pre - deformation
Pre - deformed by pps

Figure 6

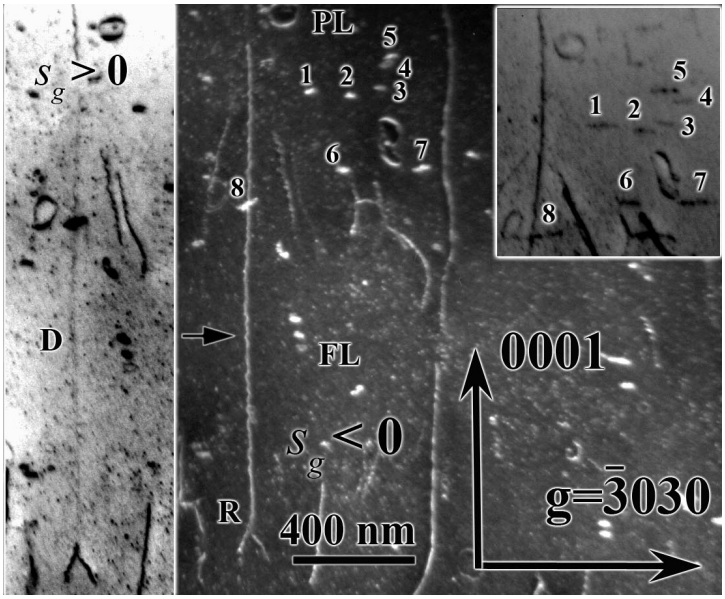

Figure 7

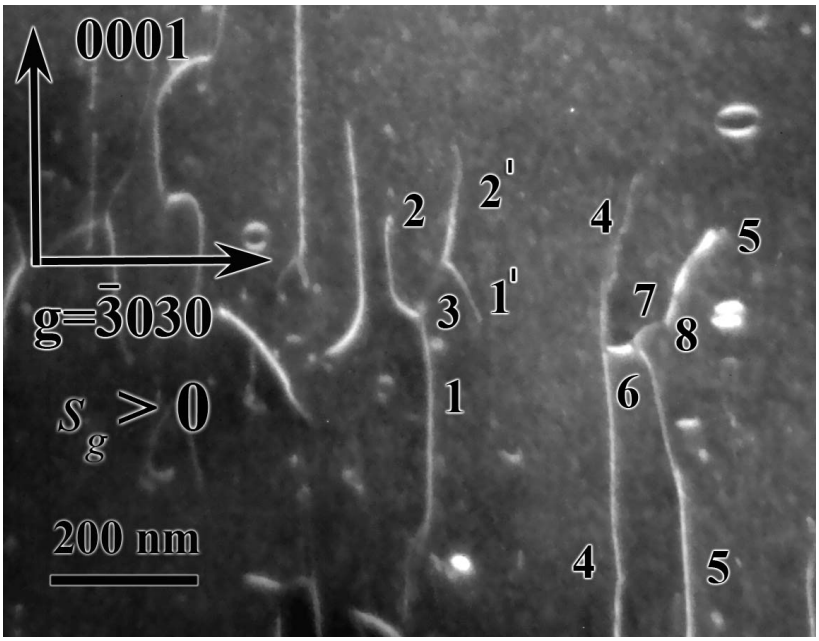

Figure 8a

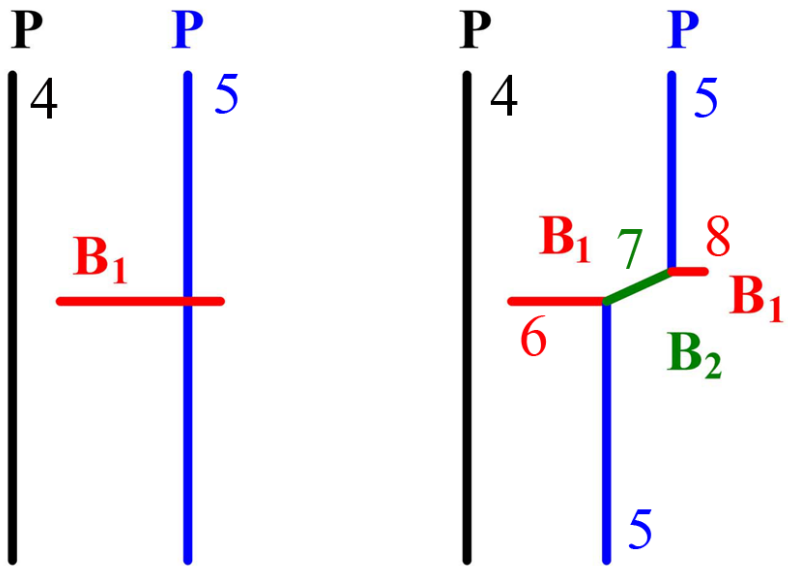

Figure 8b

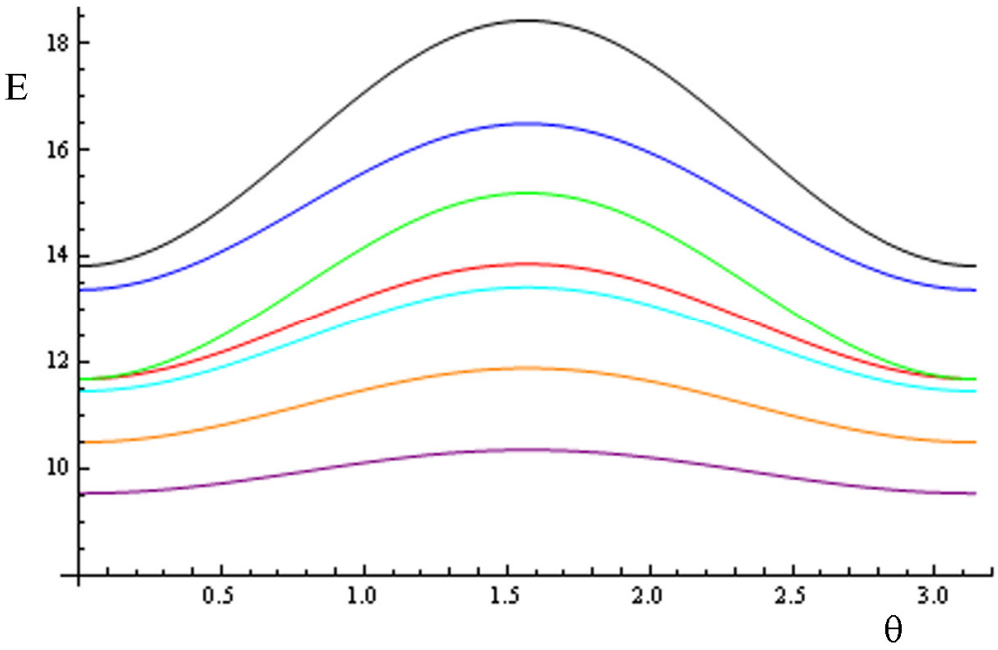

Figure A-1